Korean J. Chem. Eng., 36(9), 1509-1517 (2019)
DOI: 10.1007/s11814-019-0342-7

pISSN: 0256-1115
eISSN: 1975-7220

Fluorescence detection of bisphenol A in aqueous solution using magnetite core-shell material with gold nanoclusters prepared by molecular imprinting technique

Dasom Kim and Byunghwan Lee†

Department of Chemical Engineering, Keimyung University, 1095 Dalgubeoldaero, Dalseo-gu, Daegu 42601, Korea
(*Received 11 February 2019 • accepted 15 July 2019*)

Abstract−Technologies for detecting endocrine disrupting compounds such as bisphenol A (BPA) in an aqueous solution in a convenient way and low cost have gained much attention. In this work, to overcome the drawbacks of current detection methods, we applied molecular imprinted polymers (MIPs) to core-shell materials. The core-shell material has the advantage that both properties of the core and shell materials can be used simultaneously. After binding BPA in an aqueous solution, the magnetic core material was able to be recovered using magnetism. In addition, functional groups were easily introduced using silica as a shell material. Gold nanoclusters (AuNCs) and MIPs were used to give changes in the fluorescence intensity when BPA was bound to the prepared core-shell material. The physical properties of the prepared Fe_3O_4@SiO_2@AuNCs-MIP (CS-MIP) were analyzed and fluorescence intensities of CS-MIP for BPA were examined. The prepared material was recovered using a magnet, and the recovered CS-MIP was regenerated to investigate how the fluorescence properties for BPA changed in the subsequent reuses.

Keywords: Bisphenol A, Fluorescence, Detection, Core-shell, Molecular Imprinting

INTRODUCTION

Recent industrial development has raised concerns about endocrine disrupting compounds (EDCs) released into the water environment. In particular, EDCs in effluent from industrial wastewater treatment plants are causing frequent water pollution problems. EDCs have a molecular structure similar to sex steroids secreted in vivo and may act like sex hormones [1]. These substances are known to induce deterioration of human reproductive function, malformations, growth disorders, cancer and the like. Recent studies have shown that approximately 800 chemicals are classified as EDCs, which include DDT, dioxins, polychlorinated biphenyls, phthalates, bisphenol A, polyphenyl ethoxylates, and heavy metals [2-4].

Bisphenol A (BPA), one of the EDCs, is an organic compound made by the condensation of one molecule of acetone and two molecules of phenol. BPA has been used as a raw material for epoxy resin, which has been mainly used for compact discs, automobile parts, baby bottles, plastic bowls, receipts, food cans, and dental resins. BPA has a molecular structure similar to that of estrogen, disturbing the endocrine system in the human body [5]. For this reason, it is necessary to detect and remove trace amounts of BPA in water.

Several methods have been used to detect EDCs, such as BPA in aqueous solution. First methods are mass spectrometry based techniques such as gas chromatography, liquid chromatography, and inductively coupled plasma analysis [6,7]. Mass spectrometry provides a high degree of accuracy in analysis, but requires a high level of equipment cost and is difficult to operate because of the requirement of the high level of proficiency in operation. In addition, it takes a long time to analyze and cannot be used easily and quickly on-site due to its large size [8]. The second one is an electrochemical sensor using various materials as electrodes [9]. Although research on the use of nanoporous gold as an electrode of a sensor has been carried out, metals such as gold have too high density to improve the specific surface area. In addition, due to the nature of the material, the functional groups capable of bonding to the metal surface are limited, making it difficult to fabricate a sensor [10]. Recently, graphene has been prepared by chemical synthesis, and its application as a sensor electrode is underway [11]. Graphene has the advantages of easy functionalization, mass production and large surface area. However, it has relatively low sensitivity and selectivity when applied to electrochemical sensors in aqueous solution [12]. Third, there is a color sensor, which is a simple way to detect pollutants in the field [13]. The color sensor uses color change due to the agglomeration of nanoparticles such as gold, or color change due to the combination of organic dyes and analytes [14]. Color sensors have the advantage of fast and simple analysis, but they are difficult to reuse [15,16].

To overcome the drawbacks of current detecting methods, we used core-shell material as a fluorescence sensor for BPA in aqueous solution in this work. Core-shell material consists of a structure in which the core material is surrounded by the shell material. Depending on the core and shell materials used, various combinations of forms can be made [17]. This makes it possible to produce various properties such as magnetic, fluorescence, acid resistance, abrasion resistance, and so on, giving high applicability to various fields [18]. Core-shell materials have been actively studied, mainly in drug delivery media, magnetic resonance imaging, cell separation, immunoassay, catalysis, and optics [19]. Recently, core-shell material was used to adsorb and remove BPA in aqueous solution [20] or to investigate adsorption of some target compounds in aque-

†To whom correspondence should be addressed.
E-mail: leeb@kmu.ac.kr

ous solution [21].

We used Fe_3O_4 as a core material. Fe_3O_4 is is easy to prepare, is inexpensive, and can be recovered easily using magnetic property. Methods for preparing Fe_3O_4 include solvothermal synthesis and coprecipitation [18]. In this work, Fe_3O_4 particles with small particle size were prepared by coprecipitation method. Silica was used as a shell material. Silica can bind various functional groups to the surface by the large amount of hydroxyl groups [22]. Gold nanoclusters (AuNCs) were bound to the prepared core-shell material, Fe_3O_4@SiO_2. AuNCs have strong luminescence emission characteristics by aggregation-induced emission, small size, easy preparation condition, and non-toxicity. In addition, they exhibit a strong and durable fluorescence signal superior to other quantum dots attributable to better resistance to photobleaching and blinking [23]. Due to these properties, AuNCs are attracting much attention as ideal fluorescence sensors and are used as sensors in various fields, such as selective detection of Hg^{2+} ions and glucose [24-26]. Recently, it has been proposed to use an electrochemical sensor using a glassy carbon electrode composed of stacked graphene nanofibers and gold nanoparticles to measure BPA [20].

Sensors utilizing molecular imprinted polymers (MIPs) and gold nanoparticles have been also reported [27]. Molecular imprinting is known to memorize the shape, size, and functional groups of a template molecule and to create a corresponding bond site [28]. MIPs are synthesized through copolymerization of functional monomers and crosslinkers in the presence of template molecules [29]. MIPs have advantages such as low cost, easy synthesis, high selectivity, and high stability compared with other recognition systems, and they have been studied in many fields such as solid-phase extraction, chromatographic separation, and selective adsorption in chemical and biological sensors [30-32]. However, MIPs have disadvantages such as incomplete removal of template molecules, low binding amount, and irregular particle shape [33]. In recent years, a magnetic MIP has been developed that is both magnetic and capable of molecular recognition to easily separate BPA and its analogues from solution [34,35]. Surface molecular imprinted polymer on the core-shell particle was used in this work because it has advantages over conventional MIPs such as perfect template molecule removal, easy recombination of template molecules, and reusability [33].

To overcome the disadvantages of the above-mentioned detection methods, such as non-reusability, long analysis time, expensive equipment, and low selectivity, the core-shell material incorporating the molecular imprinting technique was prepared. It was used for fluorescence detection of BPA, one of the representative EDCs. The Fe_3O_4@SiO_2@AuNCs-MIP was prepared by bonding AuNCs to the core-shell particle surface and applying molecular imprinting technique. For comparison, Fe_3O_4@SiO_2@AuNCs-NIP with non-imprinted polymer without template molecules was also prepared. The prepared materials were magnetically recovered after use, and the change of detection efficiency after reuse was also examined.

EXPERIMENTAL

1. Materials

To prepare the core material (Fe_3O_4), we used ferrous chloride ($FeCl_2{\cdot}4H_2O$, Sigma-Aldrich, ≥99.0%, Germany), ferric chloride ($FeCl_3{\cdot}6H_2O$, Sigma-Aldrich, 97%, USA), distilled water, ammonium hydroxide solution (NH_4OH, Daejung, 25.0-28.0%, Korea), sodium citrate ($C_6H_5NaO_7{\cdot}2H_2O$, Sigma-Aldrich, ≥99.0%, Belgium) and acetone (C_3H_6O, Daejung, 99.5%, Korea).

To prepare the core-shell material (Fe_3O_4@SiO_2), we used hydrochloric acid (HCl, Samchun, 35.0-37.0%, Korea), ethanol (C_2H_5OH, Daejung, ≥95%, Korea), tetraethoxysilane (TEOS; $Si(OC_2H_5)_4$, Sigma-Aldrich, 98%, China), and (3-aminopropyl)trimethoxysilane (APTMS; $H_2N(CH_2)_3Si(OCH_3)_3$, Sigma-Aldrich, 97%, Germany).

To fabricate core-shell material incorporated with gold nanoclusters (Fe_3O_4@SiO_2@AuNCs), we used chloroauric acid ($HAuCl_4$, Sigma-Aldrich, ≥99.9%, USA), L-glutathione reduced (GSH; $C_{10}H_{17}N_3O_6S$, Sigma-Aldrich, ≥98.0%, Japan), 1-(3-dimethylaminopropyl)-3-ethylcarbodiimide hydrochloride (EDC; $C_8H_{17}N_3{\cdot}HCl$, Sigma-Aldrich, ≥98.0%, UK), 2-morpholino-ethanesulfonic acid (MES; $C_6H_{13}NO_4S$, Sigma-Aldrich, ≥99%, USA), 1-hydroxy-5-pyrrolidinedione (NHS; $C_4H_5NO_3$, Sigma-Aldrich, 98%, Japan), and phosphate buffered saline (PBS; Sigma-Aldrich, USA).

Fabricating the core-shell material with MIPs (Fe_3O_4@SiO_2@AuNCs-MIP) involved using bisphenol A (BPA; $(CH_3)_2C(C_6H_4OH)_2$, Sigma-Aldrich, ≥99%, USA), methyl alcohol (CH_3OH, Samchun, 99.5%, Korea), and acetic acid (CH_3COOH, DC chemical, 99.5%, Korea).

For fluorescence experiments, hydroquinone ($C_6H_4(OH)_2$ DC chemical, 99.0%, Korea), benzoic acid ($C_7H_6O_2$, Samchun, 99.0%, Korea), and salicylic acid ($C_7H_6O_3$, Duksan, 99.5%, Korea) were used.

2. Syntheses

2-1. Fe_3O_4

Coprecipitation method was used to make Fe_3O_4 particles with a size of about 10 nm [36]. Ferrous chloride (0.994 g) and ferric chloride (1.622 g) were dissolved in distilled water (40 mL) in a three-neck flask, and 28 wt% ammonium hydroxide solution (5 mL) serving as a reducing agent was added thereto. The mixture was stirred for 10 minutes using a motor agitator. To obtain uniform Fe_3O_4 particles, sodium citrate (4.4 g) was added, the temperature was raised to 90 °C, and the mixture was stirred for 30 minutes. After the solution was cooled to room temperature, the solid material was separated from the solution using neodymium magnet. The isolated black solid was washed twice with acetone to remove unreacted citrate. The washed material was vacuum dried at room temperature to obtain Fe_3O_4 in the form of a black powder.

2-2. Fe_3O_4@SiO_2-NH_2

The process of applying the silica shell to the prepared Fe_3O_4 core material was carried out according to the literature [22]. Fe_3O_4 (2.0 g) was mixed with 0.1 M HCl aqueous solution (100 mL) and ultrasonically dispersed for 30 minutes to modify the surface of the Fe_3O_4. The separated Fe_3O_4 was washed twice with distilled water and ethanol, respectively. The washed material was separated and placed in a three-necked flask. Ethanol (160 mL), distilled water (40 mL), ammonium hydroxide solution (5 mL) and TEOS (5 mL) were added to the beaker and stirred vigorously. The stirred mixture was added to the three-necked flask containing Fe_3O_4 and stirred for 12 hours. The reacted material was separated and washed three times with distilled water. The material was vacuum dried at 60 °C for 12 hours to obtain Fe_3O_4@SiO_2 in black powder form.

The prepared material was washed three times with distilled water and then placed in a three-necked flask. Ethanol (50 mL) and APTMS (5 mL) were added thereto, followed by stirring under a nitrogen atmosphere for 12 hours. When the reaction was completed, the material was separated and washed five times with ethanol. The material was vacuum dried at 60 °C for 12 hours to obtain Fe_3O_4@SiO_2-NH_2 in the form of a black powder.

2-3. Fe_3O_4@SiO_2@AuNCs

Distilled water (174 mL), 20 mM $HAuCl_4$ aqueous solution (20 mL), and 100 mM GSH (6 mL) were mixed at room temperature. The mixture was stirred at 70 °C for 24 hours to obtain AuNCs functionalized with carboxyl groups, and the prepared material was refrigerated at 4 °C. Fe_3O_4@SiO_2@AuNCs was prepared according to the literature [37]. EDC (20 mg) was dissolved in 0.1 mM MES (20 mL, pH 5.2), and NHS (10 mg) was dissolved in distilled water (10 mL) in another beaker. The EDC solution (6 mL) and the solution containing the carboxyl group-functionalized AuNCs prepared above (10 mL) were mixed together and stirred for 10 minutes. The color of the solution changed from light yellow to slightly hazy yellow. NHS solution (6 mL) was added to this mixture and stirred for 10 minutes. While the mixture was stirred, Fe_3O_4@SiO_2-NH_2 (60 mg) and 0.1 mM MES (50 mL, pH 5.2) were added to a three-necked flask and ultrasonically dispersed for 30 minutes. Thereafter, the stirred mixture was dropped into a three-necked flask. The mixture was stirred in the dark for 12 hours. After stirring, the prepared material was separated using neodymium magnets. The unreacted AuNCs were removed by washing three times with 0.01 M PBS solution (pH 7.0). Upon completion of the washing process, Fe_3O_4@SiO_2@AuNCs was obtained.

2-4. Fe_3O_4@SiO_2@AuNCs-MIP (or CS-MIP)

MIP layer was formed on the surface of Fe_3O_4@SiO_2@AuNCs by copolymerization process using APTMS as a functional monomer and TEOS as a crosslinking agent. BPA (2.28 mg) and APTMS (155 μL) were added to a vial and pre-polymerized for 12 hours. Fe_3O_4@SiO_2@AuNCs prepared (60 mg) was ultrasonically dispersed in 0.01 M PBS aqueous solution (40 mL, pH 7.0) for 30 minutes. After dispersion was completed, the prepolymerized BPA solution (155 μL) was added dropwise to the mixture, followed by stirring for 30 minutes. When stirring was completed, ammonium hydroxide solution (100 μL) and TEOS (80 μL) were added in this order and stirred for 12 hours. To remove the template molecule BPA, methanol (90 mL) and acetic acid (10 mL) were added to the prepared material, and the mixture was stirred for 24 hours. After stirring was completed, the separated material was vacuum dried for 12 hours to obtain Fe_3O_4@SiO_2@AuNCs-MIP. All processes were carried out in the same manner without adding BPA as a tem-

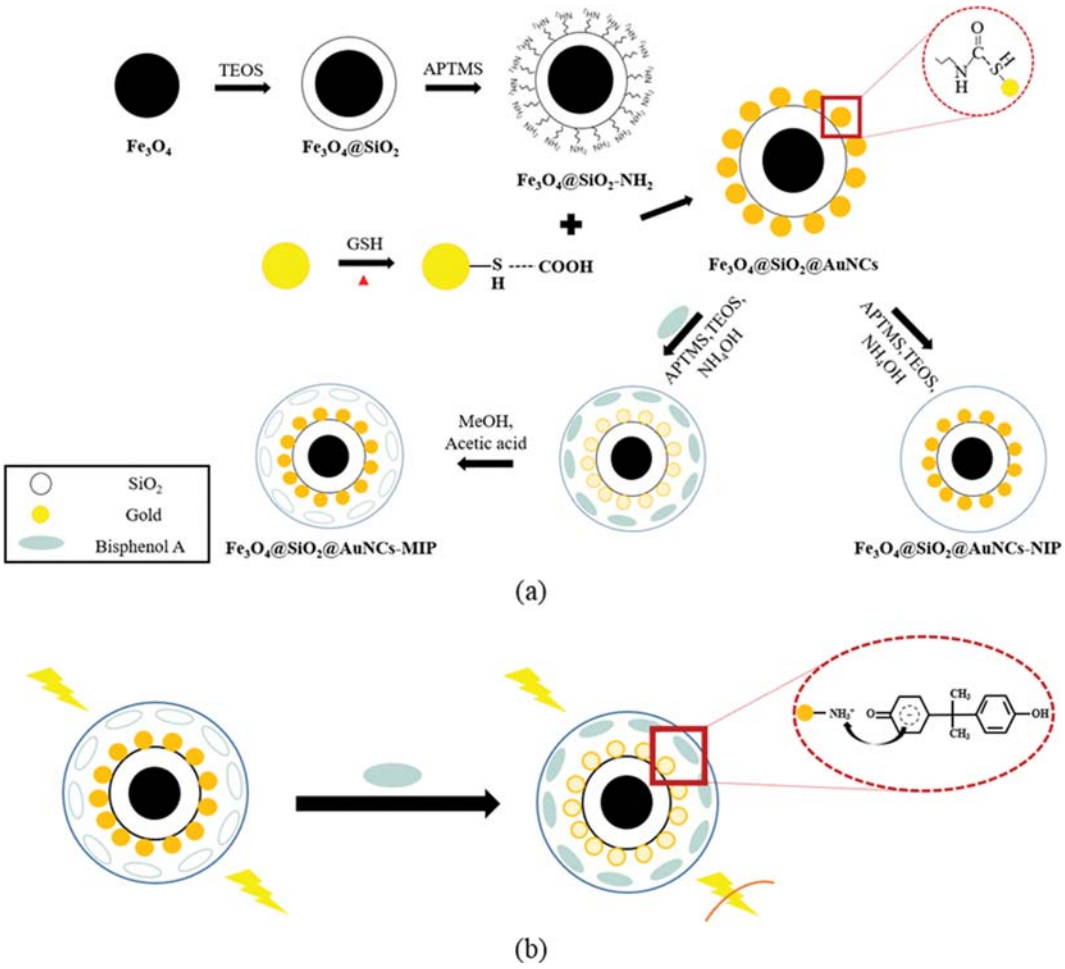

Fig. 1. (a) Synthetic procedure of Fe_3O_4@SiO_2@AuNCs-MIP (or CS-MIP) and (b) the schematic of the fluorescence quenching mechanism.

plate molecule to prepare Fe_3O_4@SiO_2@AuNCs-NIP. Subsequently, these materials were referred to as CS-MIP and CS-NIP, respectively, for simplicity. All synthetic procedures are shown in Fig. 1(a).

3. Characterization

A field emission scanning electron microscope (FE-SEM, Hitachi, Miniflex 600) was used to confirm the shape and size of the prepared material. The cross-sectional structure of the sample was analyzed using a field emission transmission electron microscope (FE-TEM, Jeol, JEM-2100F) to confirm the formation and morphology of the silica shell in the prepared material. Fourier-transform infrared spectroscopy (FTIR, Jasco, FT/IR-620V) was used to analyze the functional groups contained in the materials. A vibration sample magnetometer (VSM, LakeShore, 7407-S) was used to measure magnetic properties of the prepared materials.

4. Fluorescence Experiment

Fluorescence experiments were used to investigate the binding of BPA present in aqueous solution to CS-MIP. CS-MIP was added to the aqueous solution of BPA, and then fluorescence was measured by fluorescence-lifetime imaging microscopy (FLIM, PicoQuant, Microtime-200). Fluorescence decreased when BPA bound to the prepared CS-MIP. Fluorescence decreases as a strong charge transfer occurs between the electron-rich aromatic ring in BPA and the electron-deficient amine groups in AuNCs [37,38]. All fluorescence intensity measurements in the experiment were performed under the same conditions. In the fluorescence spectrometer, a slit for controlling the excitation wavelength and the emission wavelength fluorescence intensity was fixed at 5 nm. The excitation wavelength was set to 360 nm, the emission range was 400 nm to 700 nm, and the photomultiplier tube voltage was set to 700 V to amplify the photocurrent. Fluorescence experiments were performed varying reaction time, BPA concentrations, and target substances. The possibility of reusing the material was also investigated.

Fluorescence experiments were performed to determine the time at which the reaction of BPA with the prepared core-shell material reached equilibrium. CS-MIP (2.5 mg) was mixed with 10 μM BPA solution (100 mL) and shaken. Fluorescence was measured by extracting 1 mL of each solution at 5, 10, 20, 30, and 40 minutes, respectively, while shaking the solution. The experiment was carried out in the same way using CS-NIP.

Experiments were also conducted to investigate the fluorescence changes of CS-MIP with changes in BPA concentrations. CS-MIP (2.5 mg) was suspended in BPA aqueous solutions (100 mL) of 1, 2, 5, 7, and 10 μM, respectively, and shaken for 30 minutes. The solution (1 mL) was extracted and the fluorescence of the aqueous solution was measured. In addition, to determine the equilibrium adsorption relationship between CS-MIP and aqueous BPA solution, the concentration of each solution was measured using UV-vis spectrophotometer (Shimadzu, UV-1650). The experiments were carried out in the same way using CS-NIP.

To investigate the selectivity of the prepared material to BPA, fluorescence experiments were performed with various target substances. Hydroquinone, benzoic acid, and salicylic acid, having a molecular structure similar to that of BPA, were used to prepare 10 μM aqueous solutions. CS-MIP (2.5 mg) was suspended in each target substance aqueous solution (100 mL) and shaken for 30 minutes. The reaction-completed aqueous solution (1 mL) was extracted and fluorescence was measured. The experiment was carried out in the same way using CS-NIP.

Experiments were conducted to investigate the reusability of the prepared core-shell material. CS-MIP (2.5 mL) was mixed with 10 μM BPA solution (100 mL) and shaken for 30 minutes. The reaction-completed aqueous solution (1 mL) was extracted and fluorescence was measured. After completion of the reaction, CS-MIP was separated using the neodymium magnet. To remove BPA,

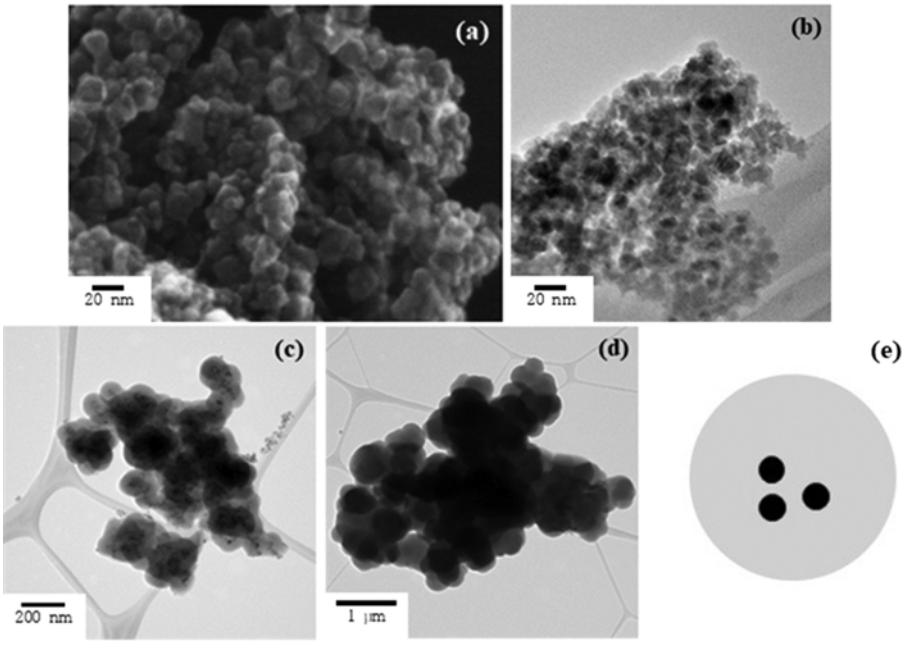

Fig. 2. (a) SEM image of Fe_3O_4, TEM images of (b) Fe_3O_4, (c) Fe_3O_4@SiO_2-NH_2, and (d) CS-MIP, and (e) the schematic of the core-shell materials prepared in this work showing nanoparticle clusters coated by single shell material.

methanol (90 mL) and acetic acid (10 mL) were added, and the mixture was stirred for 24 hours. After stirring, the CS-MIP was separated using a magnet and vacuum dried at room temperature for 12 hours. Fluorescence measurement experiments were performed in the same manner using the recovered CS-MIP. This process was repeated five times.

RESULTS AND DISCUSSION

1. Characterization

The prepared Fe_3O_4 had a black powder form. FE-SEM was used to observe the size and shape of Fe_3O_4 prepared (Fig. 2(a)). It was confirmed that the prepared Fe_3O_4 had spherical shape of about 4-10 nm. Fe_3O_4 with nanoparticle size was able to be obtained by coprecipitation [36]. As shown in Fig. 2(a), the prepared Fe_3O_4 nanoparticles aggregated with each other, which is thought to be due to the increase of the surface energy of the nanoparticles and the magnetic properties of Fe_3O_4 nanoparticles.

The prepared Fe_3O_4 nanoparticles were coated with silica shell materials. The prepared Fe_3O_4@SiO_2 was in the form of a blackish brown powder. FE-TEM was used to confirm the size and shape of Fe_3O_4, Fe_3O_4@SiO_2-NH_2, and CS-MIP prepared. In Fe_3O_4@SiO_2-NH_2 and CS-MIP, the core was surrounded by the shell material, and the TEM was used to confirm their cross-sections (Fig. 2). The prepared Fe_3O_4 nanoparticles were 4-10 nm in diameter and were clustered due to magnetic property (Fig. 2(b)). In Fe_3O_4@SiO_2-NH_2, it was confirmed that Fe_3O_4, which was a core material, was surrounded by SiO_2 as a shell material (Fig. 2(c)). The particle size of Fe_3O_4@SiO_2-NH_2 was about 100-150 nm. Core-shell particles are most common in which simple spherical core particles are completely coated with the shell of another material. However, various other types of core-shell particles have also been prepared [17]. The core-shell particles prepared in this work showed that the shell material surrounded many small core particles as shown in Fig. 2(e). The particle size of CS-MIP with gold nanoparticles and molecular imprinted polymer (MIP) layer on Fe_3O_4@SiO_2-NH_2 surface was approximately 550-600 nm (Fig. 2(d)).

FTIR analysis was performed to determine whether the samples were properly fabricated by examining the functional groups present in the prepared materials. The results are shown in Fig. 3. Analyses of Fe_3O_4, Fe_3O_4@SiO_2-NH_2, and CS-MIP samples confirmed the Fe-O peak as the major peak of Fe_3O_4 at around 587 cm^{-1} [39]. This implies that Fe_3O_4 was successfully prepared and the prepared Fe_3O_4 was included as a core material even after the silica shell material and molecular imprinted polymer was coated thereafter [40]. Si-O-Si vibration and stretching peak, which was the main peak of SiO_2, was observed at 1,095 cm^{-1} after the silica shell was coated on the Fe_3O_4 core (Fig. 3(b) and Fig. 3(c)) [37]. This indicated that Fe_3O_4 was successfully coated with silica. In addition, amine groups were confirmed in Fe_3O_4@SiO_2-NH_2 and CS-MIP via NH peaks at 3,078 cm^{-1}, 3,413 cm^{-1} and 1,643 cm^{-1} (Fig. 3(b) and Fig. 3(c)) [37]. CH_2-SH peak was confirmed at 785 cm^{-1} in CS-MIP, indicating that GSH, which was used to functionalize the gold with a carboxyl group, was included in CS-MIP (Fig. 3(c)) [41]. In CS-MIP, peptide bond peaks were also confirmed at 1,554 cm^{-1} and 1,411 cm^{-1}, which were formed by binding of amine groups of Fe_3O_4@SiO_2-NH_2 to carboxyl groups of gold surface (Fig. 3(c)) [37]. This indicated that AuNCs bound to GSH were successfully bound to the silica surface by the peptide bond formation in CS-MIP.

VSM was used to investigate the change of magnetism by the introduction of silica and molecular imprinted polymer as a shell material, and the results are shown in Fig. 4. The saturation magnetization values were 59.2 emu/g, 55.6 emu/g, and 9.87 emu/g for Fe_3O_4, Fe_3O_4@SiO_2-NH_2, and CS-MIP, respectively. The magnetic saturation values of Fe_3O_4@SiO_2-NH_2 and CS-MIP were lower than that of Fe_3O_4. This is due to the reduction of the magnetic properties of Fe_3O_4 by the coating of silica and molecular imprinted polymer in Fe_3O_4@SiO_2-NH_2 and CS-MIP. The magnetic saturation value of CS-MIP was not large, but the value was sufficient to be able to separate CS-MIP in the aqueous solution by using neo-

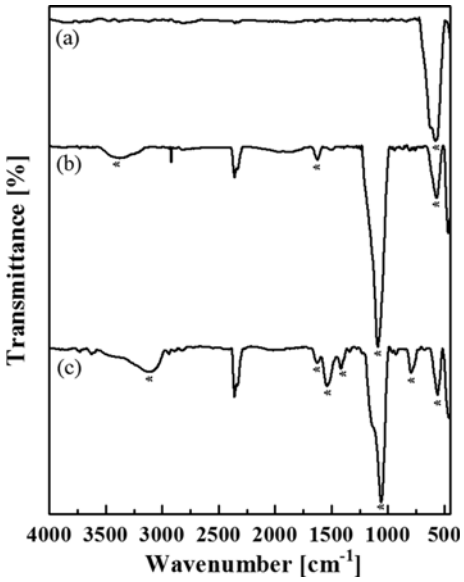

Fig. 3. FTIR spectra of (a) Fe_3O_4, (b) Fe_3O_4@SiO_2-NH_2, and (c) CS-MIP.

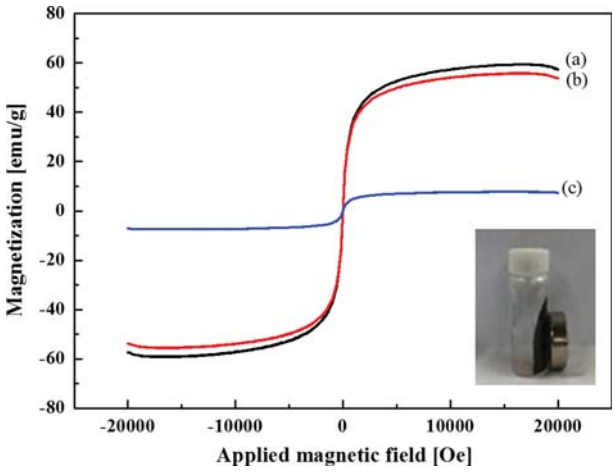

Fig. 4. Magnetization curves of (a) Fe_3O_4, (b) Fe_3O_4@SiO_2-NH_2 and (c) CS-MIP. The inset shows photographic image of CS-MIP behavior in a magnetic field.

Table 1. Correlation between magnetization and shell thickness of the prepared materials

Sample	Saturation magnetization value [emu/g]	Shell thickness[a] [nm]
Fe_3O_4	59.2	-
Fe_3O_4@SiO_2-NH_2	55.6	60.5
CS-MIP	9.87	320.4

[a]Shell thickness values were obtained from TEM images

dymium magnet as shown in the inset of Fig. 4. The correlation between the magnetic saturation value and shell thickness is shown in Table 1. In general, magnetization is reduced by combining other non-magnetic materials on the surface of the magnetic sample [42]. The relative magnetic saturation value of the Fe_3O_4@SiO_2-NH_2 to CS-MIP was 5.63, and the relative shell thickness of CS-MIP to Fe_3O_4@SiO_2-NH_2 was 5.30. As a result, it was found that the magnetic saturation value and the shell thickness were inversely proportional to each other.

2. Fluorescence Experiment

In this work, fluorescence experiments were carried out to investigate the change of fluorescence properties of CS-MIP to detect BPA in aqueous solution. As mentioned, quenching is that the intensity of the fluorescence of gas or solution is reduced due to the addition of other substances [43]. Fluorescence reduction can occur in various processes such as excited state reactions, energy transfer, complex formation, and collisional quenching, and is accompanied by dynamic fluorescence reduction or static fluorescence reduction [43]. Dynamic fluorescence reduction occurs when an excited fluorophore collides with an atom or molecule that can facilitate the transition to ground state. Static fluorescence reduction is a phenomenon in which the fluorophore forms a stable complex with other molecules at the ground state [43]. Fluorescence characteristics are represented by the Stern-Volmer equation as [44-46].

$$\frac{F_0}{F} = 1 + K_{SV} C_q \quad (1)$$

where F_0 is the fluorescence intensity in the absence of the fluorescence reduction substance, F is the fluorescence intensity in the presence of the fluorescence reduction substance, K_{SV} is the Stern-Volmer constant, and C_q is the concentration of the fluorescence reduction substance. Therefore, the amount of fluorescence reduction can be represented by $(F_0/F)-1$.

If the BPA in the aqueous solution is bound to CS-MIP, the electrons in BPA are transferred to the amine groups on the AuNCs surface, forming the Meisenheimer complex [47,48]. The Meisenheimer complex is a 1 : 1 reaction product between a group with an electron withdrawing and an aromatic hydrocarbon with a nucleophile. The photo-induced energy of AuNCs is transferred to this Meisenheimer complex, resulting in the fluorescence quenching of AuNCs [37]. Fluorescence can be reduced by the complex formation between the AuNCs, a fluorescent material, and the fluorescence-reducing material such as BPA (Fig. 1(b)). In addition, this reaction can be attributed to the static fluorescence reduction. In this work, fluorescence experiments were performed with varying reaction time, BPA concentrations, and the type of target materials. In addition, reuse experiments were conducted to confirm the reusability of CS-MIP.

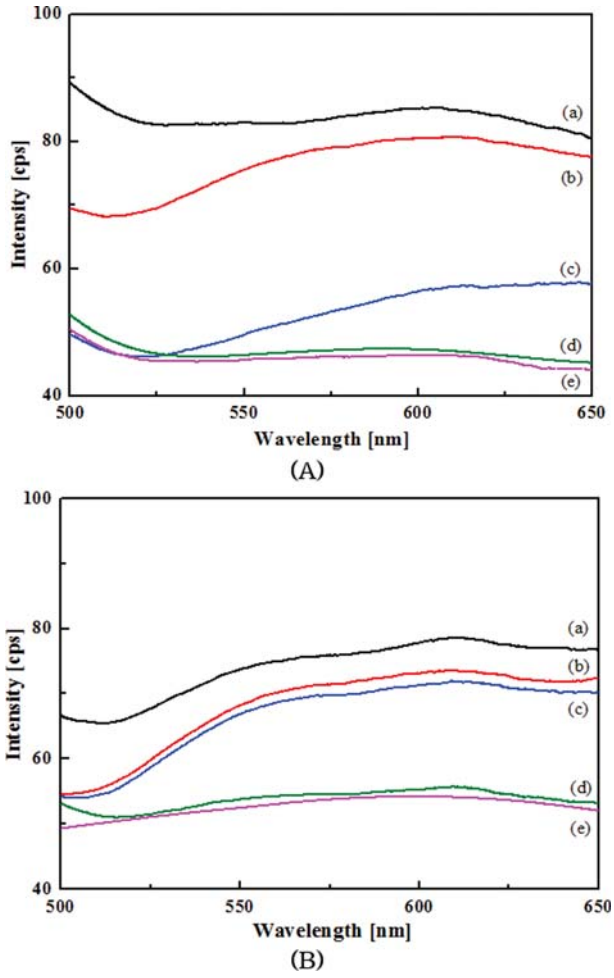

Fig. 5. Change of fluorescence intensities of (A) CS-MIP and (B) CS-NIP with time: (a) 5 minutes, (b) 10 minutes, (c) 20 minutes, (d) 30 minutes, and (e) 40 minutes.

The change in fluorescence decay over time was investigated to determine the time at which the final reaction of CS-MIP and the target substance, BPA, was terminated (Fig. 5). For comparison, experiments were also carried out using CS-NIP without molecular imprinted polymers in the structure. In both CS-MIP and CS-NIP, fluorescence decreased over time. The fluorescence reduction in CS-MIP was 1.71 times greater than in CS-NIP as shown in the figure. In addition, it was confirmed that the change of fluorescence intensity was remarkably decreased after 30 minutes from the start of the reaction. Therefore in the following, all fluorescence experiments were performed by fixing the reaction time to 30 minutes.

Experiments were conducted to investigate the fluorescence changes observed in CS-MIP and CS-NIP when different concentrations of BPA were used (Fig. 6). Fluorescence changes were measured while changing the initial concentration of BPA from 0 μM to 10 μM. As shown in Fig. 6, CS-MIP and CS-NIP exhibited the highest fluorescence values at 562 nm of wavelength. As the

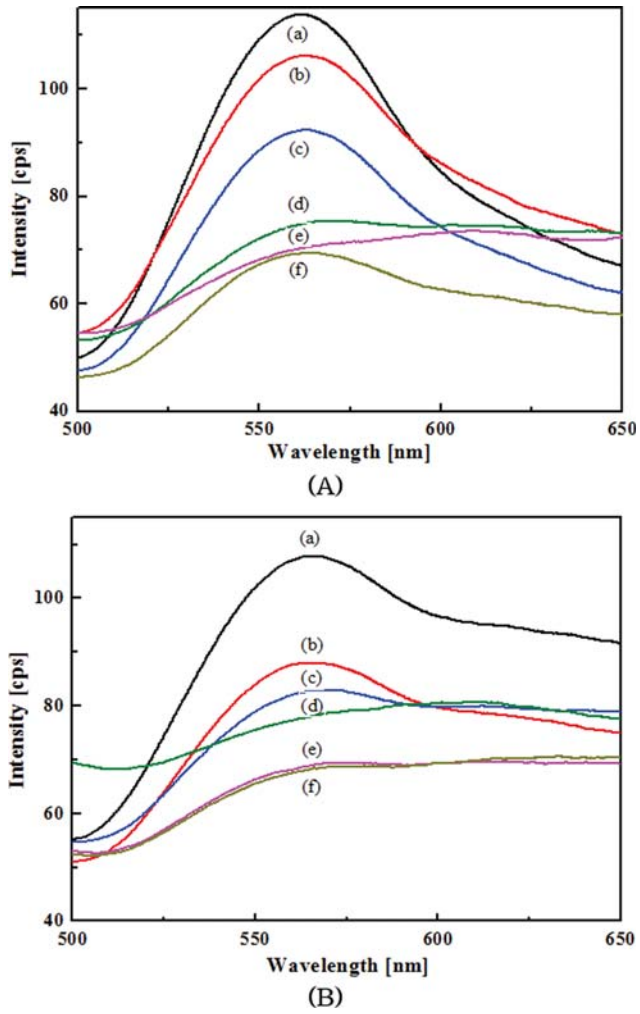

Fig. 6. Fluorescence intensity changes of (A) CS-MIP and (B) CS-NIP with the change of initial concentration of BPA: (a) 0 μM, (b) 1 μM, (c) 2 μM, (d) 5 μM, (e) 7 μM, and (f) 10 μM.

concentration of BPA in the aqueous solution increased, the fluorescence intensity decreased due to the fluorescence quenching described above. In addition, it was confirmed that CS-NIP had less fluorescence decrease than CS-MIP at the same concentration of BPA. These results suggest that larger amounts of BPA are bound to CS-MIP due to the molecular imprinting effect. In CS-MIP, BPA can bind to the molecule-imprinted site, so that the binding strength of BPA might be stronger than that of CS-NIP with no molecular imprinting.

The results of the experiments were applied to the Stern-Volmer equation, and the amount of fluorescence reduction according to BPA concentration is shown in Fig. 7. As the BPA concentration in aqueous solution increased, the amount of fluorescence reduction increased. During the increase of the BPA concentration from 0 μM to 10 μM, the amount of fluorescence reduction of CS-MIP was 0.69 compared to the initial fluorescence intensity. The amount of fluorescence reduction of CS-NIP was 0.55 under the same condition, showing that CS-MIP had greater fluorescence reduction than CS-NIP. Wu et al. also reported the detection of BPA in aqueous solution using MIP-coated gold particles.

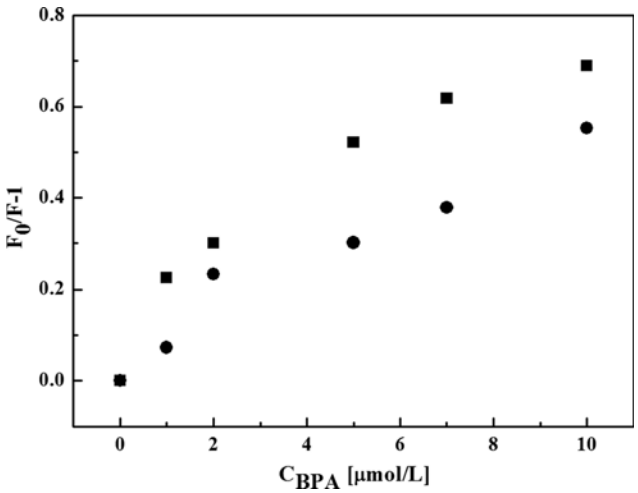

Fig. 7. Fluorescence intensity corresponding Stern-Volmer plots of CS-MIP (■) and CS-NIP (●).

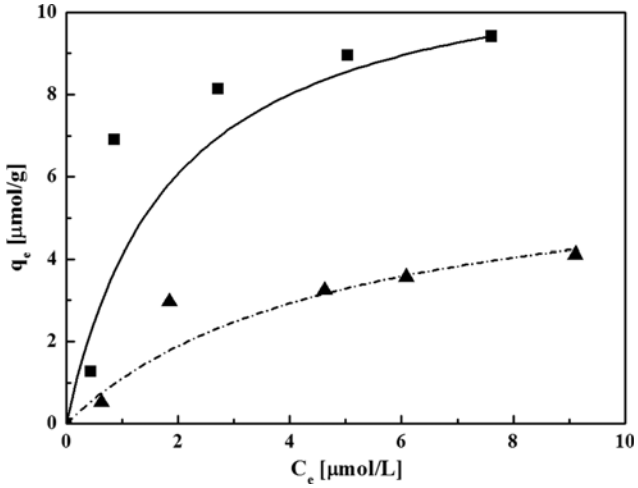

Fig. 8. Adsorption isotherms of BPA on CS-MIP (■) and CS-NIP (▲). Adsorption isotherms were obtained using Langmuir model (lines).

The detection range was 0-13.1 μM and the detection limit was 0.10 μM [37]. The CS-MIP prepared in this work showed a comparable detection range with that. However, unlike expectation, BPA concentration and fluorescence reduction did not show a complete linear relationship. Instead, it showed a similar relationship with Langmuir isotherm, so the equilibrium adsorption was investigated for the adsorption of BPA on the prepared materials.

The equilibrium adsorption amount of BPA in CS-MIP and CS-NIP was measured using UV-vis and shown in Fig. 8. As the concentration of BPA increased, the amount of BPA adsorption also increased in CS-MIP and CS-NIP. Langmuir adsorption isotherm was used to model the adsorption behavior. The Langmuir isotherm can be expressed as

$$q_e = \frac{q_m b C_e}{1 + b C_e} \quad (2)$$

where q_m is the maximum adsorption capacity (μmol/g), C_e is the

Table 2. Langmuir isotherm parameters for the adsorption of BPA by CS-MIP and CS-NIP

Sample	q_m [μmol/g]	b [L/μmol]	R^2
CS-MIP	11.74	0.535	0.868
CS-NIP	6.50	0.205	0.777

q_m: the maximum adsorption capacity
b: the Langmuir constant

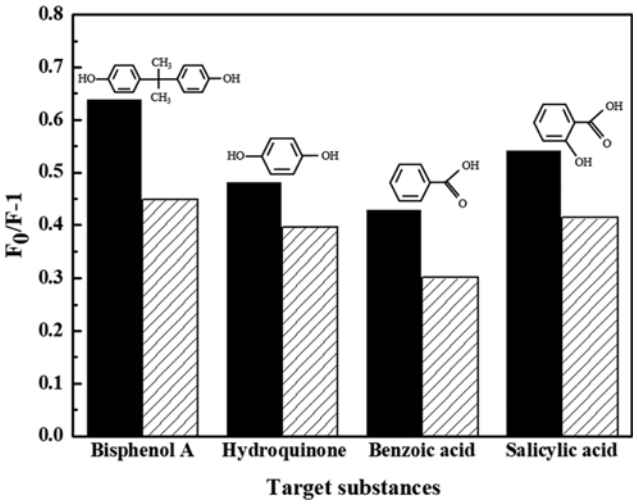

Fig. 9. Binding behaviors of different target substances at the same initial concentration on CS-MIP (■) and CS-NIP (▨).

equilibrium concentration of BPA in aqueous solution (μmol/L), and b is the Langmuir constant (L/μmol). The Langmuir isotherm assumes homogeneous surface properties and monolayer adsorption. The adsorption of BPA on the prepared materials showed high R^2 values (>0.77) and was fitted well with the Langmuir model (Table 2). The maximum amount of adsorbed BPA of CS-MIP and CS-NIP was 11.74 μmol/g and 6.50 μmol/g, respectively. In addition, CS-MIP adsorbed 1.8-times larger amounts than CS-NIP. These experimental results were in agreement with the above fluorescence experimental results.

Hydroquinone, benzoic acid, and salicylic acid were used to investigate the fluorescence response to the substances with similar molecular structure to BPA. The experimental results were applied to the Stern-Volmer equation, and the results are shown in Fig. 9. CS-MIP also showed fluorescence reduction to hydroquinone, benzoic acid, and salicylic acid, suggesting their partial conjugation with the prepared materials because of their similar molecular structure to BPA. CS-MIP showed a greater fluorescence reduction than CS-NIP for all the target substances. In addition, in both CS-MIP and CS-NIP, fluorescence intensity reduction was decreased in the order of BPA, salicylic acid, hydroquinone, and benzoic acid. Benzoic acid showed the lowest fluorescence intensity reduction. Benzoic acid has only one hydroxyl group, unlike the other materials having two hydroxyl groups. Due to the difference in the molecular structure, it seems to show a difference in the adsorption characteristics on the prepared material [49].

To investigate the reusability of CS-MIP, the fluorescence intensity of the samples was measured during the repeated experiments. BPA adsorption and fluorescence measurements, BPA desorption using methanol and acetic acid, and reuse were repeated five times. The results of the experiment are shown in Fig. 10. CS-MIP showed about 3.65% less fluorescence reduction than the first experiment when used for the second time after regeneration. It was considered that the fluorescence was changed very little and the reusability was high. However, the subsequent reuse experiments confirmed that fluorescence reduction was about 34.7% less in the fifth experiment than in the first experiment. This is presumably because the BPA bound to the CS-MIP was not completely removed during the regeneration of the CS-MIP. However, the CS-MIP was confirmed to be able to use several times through the recovery using the magnet by maintaining the constant fluorescence reduction in the five times reuse experiments.

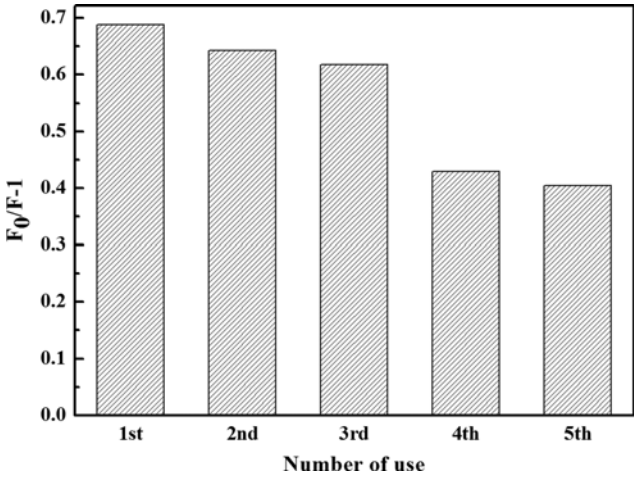

Fig. 10. Fluorescence intensity corresponding Stern-Volmer plots of CS-MIP in the regeneration experiments.

CONCLUSION

CS-MIP was prepared by grafting molecular imprinted polymers to core-shell materials to detect BPA in aqueous solution. Fe_3O_4, having a size of about 10 nm, was prepared by coprecipitation. The shell material, silica, was successfully formed on the surface of the core material, and gold particles were bonded to the core-shell material surface using amine groups and carboxyl groups. Fluorescence decreased as the reaction time with BPA in aqueous solution increased, and CS-MIP showed greater fluorescence reduction than CS-NIP. Fluorescence decreased as the concentration of BPA in aqueous solution increased, and CS-MIP showed greater fluorescence reduction than CS-NIP at the same concentrations. Hydroquinone, benzoic acid, and salicylic acid were also partially bound to CS-MIP due to their similar molecular structure to BPA, resulting in a decrease in fluorescence. However, the largest reduction in fluorescence was observed in BPA. Further studies on precise molecular imprinting seems to be needed for the selective detection of BPA. It also confirmed the possibility of detecting other target substances through molecular imprinting. In addition, it was shown that CS-MIP can be recovered and reused by using magnetism.

The fluorescence reduction was reduced by about 34.7% after five-times of reuse. If the process of removing BPA bound to CS-MIP after each fluorescence experiment is improved, the efficiency of reuse is expected to be increased. Based on these results, we think core-shell fluorescence sensor developed in this work can be applied to real wastewater.

ACKNOWLEDGEMENT

This research was supported by the Bisa Research Grant of Keimyung University in 2018.

REFERENCES

1. K. V. Thomas, M. R. Hurst, P. Matthiessen and M. J. Waldock, *Environ. Toxicol. Chem.*, **20**, 2165 (2001).
2. T. Colborn, D. Dumanoski and J. P. Myers, Our stolen future, Dutton, New York (1996).
3. G. T. Ankley, R. D. Johnson, G. Toth, L. C. Folman, N. E. Detenbeck and S. P. Bradbury, *Rev. Toxicol. Ser. B: Environ. Toxicol.*, **1**, 71 (1997).
4. R. J. Kavlock, G. P. Daston, C. Derosa, P. Fenner-Crisp, L. E. Gray, S. Kaattari, G. Lucier, M. Luster, M. J. Mac, C. Maczka, R. Miller, J. Moore, R. Rolland, G. Scott, D. M. Sheehan, T. Sinks and H. A. Tilson, *Environ. Health Perspect.*, **104**, 715 (1996).
5. K. Ahn and B. Kim, *J. Environ. Toxicol.*, **18**, 175 (2003).
6. S. M. Zimmers, E. P. Browne, P. W. Okeefe, D. L. Anderton, L. Kramer, D. A. Reckhow and K. F. Arcaro, *Chemosphere*, **104**, 237 (2014).
7. G. Shen, G. Yu, Z. X. Cai and Z. Zhang, *Chin. Sci. Bull.*, **50**, 2681 (2005).
8. R. C. Dong, J. H. Li, H. Xiong, W. H. Lu, H. L. Peng and L. X. Chen, *Talanta*, **130**, 182 (2014).
9. H. Kim and Y. Kim, *Curr. Appl. Phys.*, **9**, 88 (2009).
10. H. Kim, Y. Kim and J. Ko, *J. Korean Inst. Gas*, **12**, 32 (2008).
11. S. Stankovich, D. A. Dikin, R. D. Piner, K. A. Kohlhaas, A. Kleinhammes, Y. Jia, Y. Wu, S. T. Nguyen and R. S. Ruoff, *Carbon*, **45**, 1558 (2007).
12. W. Lian, S. Liu, J. Yu, X. Xing, J. Li, M. Cui and J. Huang, *Biosens. Bioelectron.*, **38**, 163 (2012).
13. Y. Kim, R. C. Johnson and J. T. Hupp, *Nano Lett.*, **1**, 165 (2001).
14. J. Liu and Y. Lu, *Nat. Protoc.*, **1**, 246 (2006).
15. C. Zhang and K. S. Suslick, *J. Am. Chem. Soc.*, **127**, 11548 (2005).
16. Y. Kim and B. Lee, *Korean Chem. Eng. Res.*, **49**, 393 (2011).
17. R. Chaudhuri and S. Paria, *Chem. Rev.*, **112**, 2373 (2012).
18. H. L. Ding, Y. X. Zhang, S. Wnag, J. M. Xu, S. C. Xu and G. H. Li, *Chem. Mater.*, **24**, 4752 (2012).
19. Y. Deng, D. Qi, C. Deng, X. Zhang and D. Zhao, *J. Am. Chem. Soc.*, **130**, 28 (2008).
20. Q. Zhou, Y. Wang, J. Xiao and H. Fan, *Synth. Met.*, **212**, 113 (2016).
21. X. Zhao, Y. Cai, T. Wang, Y. Shi and G. Jiang, *Anal. Chem.*, **80**, 9091 (2008).
22. Y. Deng, C. Wang, J. Hu, W. Yang and S. Fu, *Colloids Surf. A Physicochem. Eng. Asp.*, **262**, 87 (2005).
23. T. T. Chen, Y. H. Hu, Y. Cen, X. Chu and Y. Lu, *J. Am. Chem. Soc.*, **135**, 11595 (2013).
24. L. Shang, S. J. Dong and G. U. Nienhaus, *Nano Today*, **6**, 401 (2011).
25. J. P. Xie, Y. G. Zheng and J. Y. Ying, *Chem. Commun.*, **46**, 961 (2010).
26. L. H. Jin, L. Shang, S. J. Guo, Y. X. Fang, D. Wen, L. Wang, J. Y. Yin and S. J. Dong, *Biosens. Bioelectron.*, **26**, 1965 (2011).
27. J. Huang, X. Zhang, S. Liu, Q. Lin, X. He, X. Xing and W. Lian, *J. Appl. Electrochem.*, **41**, 1323 (2011).
28. J. H. Li, Z. Zhang, S. F. Xu, L. X. Chen, N. Zhou, H. Xiong and H. L. Peng, *J. Mater. Chem.*, **21**, 19267 (2011).
29. L. X. Chen, S. F. Xu and J. H. Li, *Chem. Soc. Rev.*, **40**, 2922 (2011).
30. S. Suriyanarayanan, P. J. Cywinski, A. J. Moro, G. J. Mohr and W. Kutner, *Top. Curr. Chem.*, **325**, 165 (2012).
31. Q. Yang, J. Li, X. Wang, H. Peng, H. Xing and L. Chen, *Biosens. Bioelectron.*, **112**, 54 (2018).
32. X. Wang, S. Yu, W. Liu, L. Fu, Y. Wang, J. Li and L. Chen, *ACS Sens.*, **3**, 378 (2018).
33. D. M. Gao, Z. P. Zhang, M. H. Wu, C. G. Xie, G. J. Guan and D. P. Wang, *J. Am. Chem. Soc.*, **129**, 7859 (2007).
34. Y. Ji, J. Yin, Z. Xu, C. Zhao, H. Huang, H. Zhang and C. Wang, *Anal. Bioanal. Chem.*, **395**, 1125 (2009).
35. Z. Xu, L. Ding, Y. Long, L. Xu, L. Wang and C. Xu, *Anal. Methods*, **3**, 1737 (2011).
36. N. S. Elbialy, M. M. Fathy and W. M. Khalil, *Phys. Med.*, **30**, 843 (2014).
37. X. Wu, Z. Zhang, J. Li, H. You, Y. Li and L. Chen, *Sens. Actuators B Chem.*, **211**, 507 (2015).
38. T. Htun, *J. Fluoresc.*, **14**, 217 (2004).
39. M. Yamaura, R. Camilo, L. Sampaio, M. Macedo, M. Nakamura and H. Toma, *J. Magn. Magn. Mater.*, **279**, 210 (2004).
40. J. Groen, L. Peffer and J. Perez-Ramirez, *Micropor. Mesopor. Mater.*, **60**, 1 (2003).
41. G. Socrates, Infrared Characteristic Group Frequencies, Wiley, New York (1994).
42. J. Wang, S. Zheng, Y. Shao, J. Liu, Z. Xu and D. Zhu, *J. Colloid Interface Sci.*, **349**, 293 (2010).
43. J. R. Lakowicz, Quenching of fluorescence. Principles of fluorescence spectroscopy, Springer Publications, Boston (1983).
44. B. P. Kamat and J. Seetharamappa, *J. Chem. Sci.*, **117**, 649 (2005).
45. P. P. H. Cheng, D. Silvester, G. L. Wang, G. Kalyuzhny, A. Douglas and R. W. Murray, *J. Phys. Chem. B*, **110**, 4637 (2006).
46. R. Gopal, J. K. Lee, J. H. Lee, Y. G. Kim, G. C. Oh, C. H. Seo and Y. Y. Park, *Int. J. Mol. Sci.*, **14**, 2190 (2013).
47. J. P. Colpa, C. MacLean and E. L. Mackor, *Tetrahedron*, **19**, 65 (1963).
48. T. Gunnlaugsson, P. E. Kruger, T. C. Lee, R. Parkesh, F. M. Pfeffer and G. M. Hussey, *Tetrahedron Lett.*, **44**, 6575 (2003).
49. Y.-H. Kim, B. Lee, K.-H. Choo and S.-J. Choi, *Micropor. Mesopor. Mater.*, **185**, 121 (2014).